

IQ Impairments and Corrections in Ultra-wideband transmitters

Shannon Wanner

iDirect, Herndon, VA, USA

swanner@idirect.net

Abstract — This paper addresses the implications and challenges of IQ impairments in a design of an ultra-wideband transmitter along with enhancements to corrective topologies that address the frequency dependency of IQ imbalances. The paper also addresses the environmental impact on IQ imbalances through feedback corrective methods. Varying environmental conditions are addressed through the separation of static and dynamic IQ impairments along with dynamic IQ estimation and corrective techniques.

Index Terms — Communications, Digital Pre-distortion, Transmitters, Sideband Suppression, Radar, IQ impairments, IQ compensation

I. INTRODUCTION

The increasing trend in satellites along with a need in telecom for 5G and beyond are demanding requirements for ultra-wide band carriers such as 500 Msps and 1 Gbps. The wide-band nature of these carriers are presenting new challenges in the implementation of traditional IQ modulator and DACs that once were neglected in narrow bandwidths such as the frequency dependency of gain and phase imbalances. High order mod-cods such as 256 APSK or QAM require exceptional SNR and thus self-interference introduced by image suppression and DC leakage should be kept at a minimum. The pristine needs of such carriers place stricter requirements on image suppression. To meet these suppression requirements, adaptive correction techniques are being employed in the industry. This paper strives to enhance the modeling, detection, and correction of image suppression in ultra-wide-band transmitters.

II. MATHEMATICAL FORMULATION AND PICTORIAL DEPICTIONS IQ IMPAIRMENTS

A baseband signal can be written as follows

$$y_m(t) = y_i(t) + jy_q(t), \quad (1)$$

where $y_i(t)$ and $y_q(t)$ are real and imaginary components of the signal respectively [1]. The modulator up-converts the signal to IF/RF frequency and is mathematically described as

$$y_{trans}(t) = \text{real}\{y_m(t)e^{-jw_{lo}t}\}, \quad (2)$$

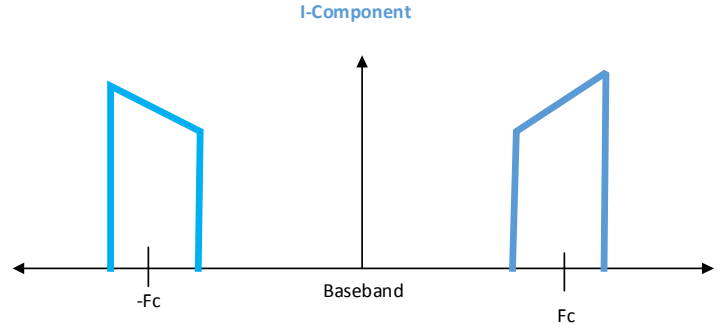


Fig. 1. Frequency Domain representation of I-component depicting an even-mode.

where w_{lo} is the RF carrier frequency generated by the modulator. The I-component of baseband signal with baseband offset frequency, w_c , can be written as

$$y_i(t) = x_i(t) \cos(w_c t) \quad (3)$$

[1]. Taking the Fourier transform of Eq. 3, results in the following

$$Y_i(w) = F\{y_i(t)\} = F\{x_i(t)\} * F\{\cos(w_c t)\} \\ = X_i(w) * F\left\{\frac{e^{jw_c t} + e^{-jw_c t}}{2}\right\}, \quad (4)$$

after manipulation, Eq. 4 results in the following

$$Y_i(w) = \frac{X_i(w)}{2} * [\delta(w - w_c) + \delta(w + w_c)]. \quad (5)$$

The Fourier transform in Eq. 5 of an even mode signal is visually depicted in Fig. 1. The Q-component of baseband signal with offset frequency, w_c , can be written as

$$y_q(t) = -x_q(t) \sin(w_c t) \quad (6)$$

[1]. Taking the Fourier transform of Eq. 6, results in

$$Y_q(w) = F\{x_q(t)\} * F\{-\sin w_c t\} \\ = X_q(w) * F\left\{\frac{e^{-jw_c t} - e^{jw_c t}}{2j}\right\}, \quad (7)$$

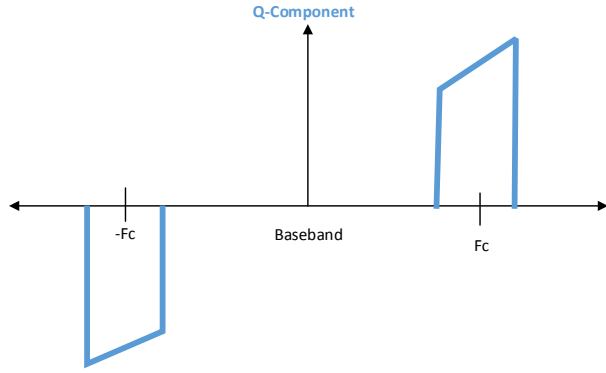


Fig. 2. Frequency Domain representation of Q-component depicting an odd-mode.

after manipulation, Eq. 7 results in

$$Y_q(w) = \frac{X_q(w)}{2j} * [\delta(w - w_c) - \delta(w + w_c)]. \quad (8)$$

The Fourier transform in Eq. 8 of an odd mode signal is visually depicted in Fig 2. A baseband signal in Eq. 2 can be reformulated as

$$y_{trans}(t) = \frac{y_m(t)}{2} e^{-jw_{lo}t} + \frac{y_m^*(t)}{2} e^{jw_{lo}t} \quad (9)$$

[1]. Substituting in I/Q components into $Y_m(w)$ and manipulating results in

$$Y_m(w) = \frac{Y_i(w)}{2} * [\delta(w - w_c) + \delta(w + w_c)] + \frac{Y_q(w)}{2} * [\delta(w - w_c) - \delta(w + w_c)]. \quad (10)$$

Taking the Fourier transform of Eq. 9 and assuming

$$Y_m(w) = Y_m^*(w), \quad (11)$$

results in the following

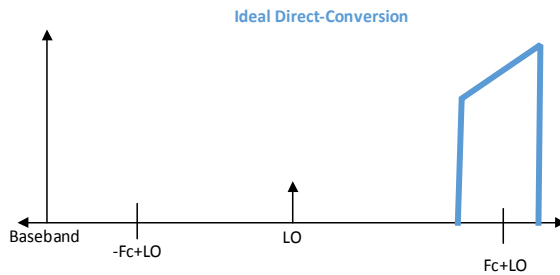


Fig. 3. Ideal direction conversion with baseband offset

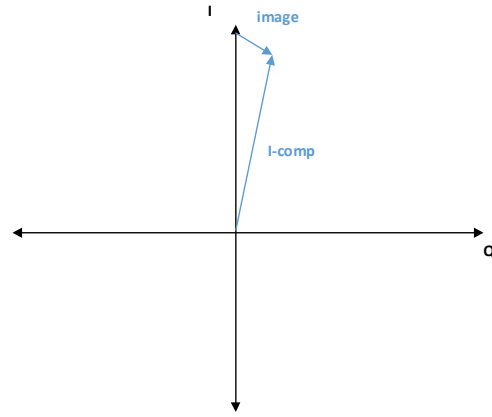


Fig. 4. I-vector, Q-vector, and image vector relationship

$$Y_{trans}(w) = \frac{Y_m(w)}{2} * [\delta(w + w_{lo}) + \delta(w - w_{lo})]. \quad (12)$$

Substituting $Y_m(w)$ into $Y_{trans}(w)$, forms the following

$$Y_{trans}(w) = \left\{ \frac{X_i(w) + X_q(w)}{4} * \delta(w - w_c) + \frac{X_i(w) - X_q(w)}{4} * \delta(w + w_c) \right\} * [\delta(w + w_{lo}) + \delta(w - w_{lo})]. \quad (13)$$

As shown in Eq. 13, the image component, $\delta(w + w_c)$, is canceled out on perfect balance of I and Q components, which is depicted in Fig. 3. Cancellation can be demonstrated by setting $x_i(t) = x_q(t)$ to a constant value, which results in a CW after modulator. The cancellation and production of an image tone can be depicted in vector form as shown in Fig. 4. Phase and amplitude imbalances between I and Q component results in an image vector.

II. IMPACT ON IMAGE-SUPPRESSION ON COMMUNICATION SYSTEMS

The impact of image suppression on communication waveforms results in self-degradation as shown in Fig. 5, when the carrier is symmetric about baseband. EVM is degraded by the presence of the image and should be modeled in analysis of system performance. Mathematically, the self-interference and Gaussian white noise, AWGN, can be combined to determine overall degradation as in the following

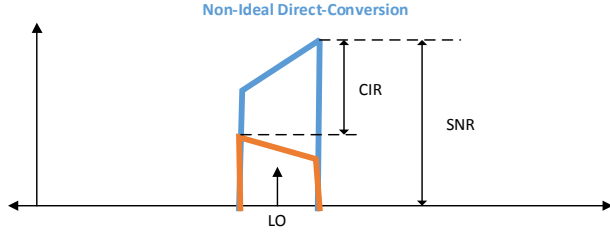


Fig. 5. Non-ideal direct conversion

$$CNIR = 10 \log_{10} \left(\left(\frac{1}{\frac{SNR_{input}}{10}} + \frac{1}{\frac{CNIR_{image}}{10}} \right)^{-1} \right), \quad (14)$$

where SNR_{input} is induced by AWGN and $CNIR_{image}$ is the self-interference induced by image carrier. The image PSD level should be kept 15 dB below the AWGN level to avoid additional degradation greater than 0.1 dB.

III. FREQUENCY IMPACT ON IQ IMBALANCES

The IQ imbalances of typical direct conversion transmitters shown in Fig. 6 can be separated into two linear components, LO dependent and LO independent components. The LO dependent components, A_{imb} and θ_{imb} , are associated with the modulator itself in the generation of orthogonal mixing tones where A_{imb} is the amplitude imbalance of the tones and θ_{imb} is the phase imbalance relative to perfect orthogonality of the mixing tones. The LO dependent component is wideband in nature as it affects the baseband frequencies components equally. The non-LO dependent components, $L_{imb}(w)$ and θ_{delay} , are IQ path dependent imbalances. The $L_{imb}(w)$ relationship to IQ filters can be further described as

$$L_{imb}(w) = L_I(w) / L_Q(w), \quad (15)$$

and is the phase and gain difference between IQ filters. The IQ filters are typically used to remove Nyquist images and spurious content generated by the DAC. θ_{delay} is related to time delay difference between the IQ paths through the

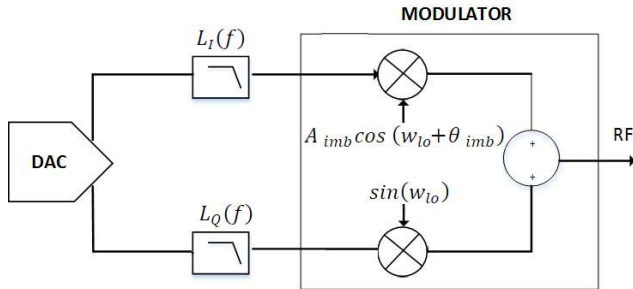


Fig. 6. Typical direct conversion transmitter implementation with amplitude and phase imbalance.

baseband frequency as described by

$$\theta_{delay} = w_{baseband} T_{delay}, \quad (16)$$

where T_{delay} is a cumulative time delay difference of digital paths, transmissions lines and IQ filters. As the imbalances operate independently on IQ branches, the gain and phase imbalances can be linearly added together to create net imbalances,

$$G_{imb}(w) = L_{imb}(w) * A_{imb} \quad (17)$$

and

$$\phi_{imb}(w) = \angle L_{imb}(w) + \theta_{imb} + \theta_{delay}. \quad (18)$$

Furthermore in most applications, it can be shown that the LO-dependent or wideband imbalances compared to non-LO or baseband dependent imbalances are more sensitive to dynamic operating conditions such as temperature. Therefore, the baseband components can be treated quasi statically. The separation of frequency dependent and LO dependent imbalances allows for separation of corrective methods and makes a corrective topology more inductive to feedback correction.

IV. CORRECTIVE TOPOLOGY

The separation of wide band and base-band components allows for separation of dynamic and quasi static correction of wide-band and base-band dependent imbalances respectively. The separation of imbalance leads to independent compensation methods. The imbalance compensation methods can happen in either a frequency or time domain topology based on the complexity of the impairment or ease of implementation. The wideband LO correction can be visually derived from Fig. 4 and shown in Fig. 7 in the time domain. The orthogonality imbalance can be described as vector through combination of a scaled Q component adding to the I component. Mathematically this

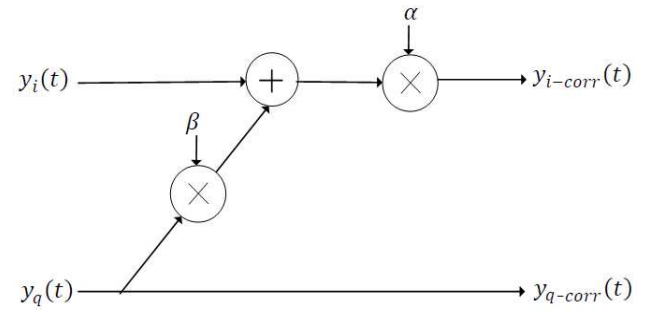


Fig. 7. Wideband corrective topology for phase and amplitude imbalances for direct conversion transmitter

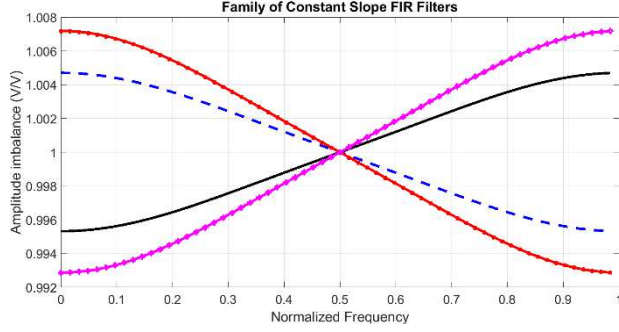


Fig. 8. Constant slope FIR filter for frequency dependent imbalance correction.

can be written as

$$y_{i-corr}(t) = \alpha\{y_i(t) + \beta y_q(t)\}, \quad (19)$$

where

$$\alpha = (1 + A_{imb})\cos(\theta_{imb}) \quad (20)$$

and

$$\beta = \sin(\theta_{imb}) \quad (21)$$

can be derived from the wide-band θ_{imb} and A_{imb} imbalances. If $\|L_{imb}(f)\|$ is well behaved and $\angle L_{imb}(f)$ is neglected, then the baseband frequency dependent gain imbalance can be compensated by using a FIR constant slope filter which may be adjusted based on calibration as shown in Fig. 8 [2]. If amplitude and phase imbalance are not well behaved over frequency, then it becomes advantageous to move the correction into the frequency domain. Taking the Fourier transform of wideband correction in Eq. 19 results in the following

$$Y_{i-corr}(w) = y_{i-corr}(t) = \alpha F\{y_i(t)\} + \alpha\beta F\{y_q(t)\}. \quad (22)$$

Thus, turning the wideband compensation method into a frequency dependent compensation. The compensation can be done in a frequency selective manner without comprising original information content.

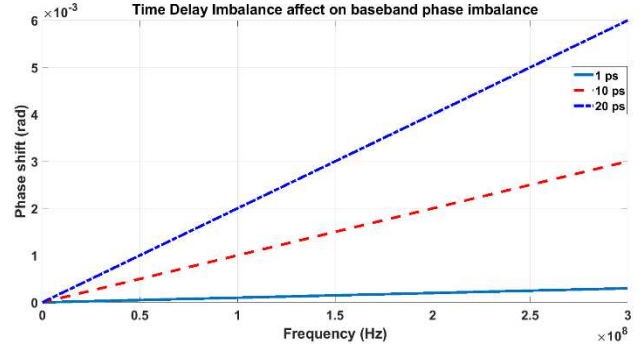


Fig. 9. Phase imbalance over baseband frequency as a result of time delay imbalance

As shown in Fig. 9, the time delay imbalance will result in a linear phase imbalance with respect to baseband frequency offset. The delay can be compensated by using integer and fractional delay filters [3]. The compensation should be in opposite direction of the average rate of change of phase vs base-band frequency offset.

VI. ADAPTIVE BLIND ESTIMATION IQ IMPAIRMENTS

Adaptive blind estimation of IQ imbalance parameters can be accomplished using feedback methods as shown in Fig. 10 and using the principle of orthogonality

$$0 = \int_{-l}^l I(t)Q(t)dt. \quad (23)$$

The orthogonality principle can be seen visually through Fig. 11. Sin and cos functions are even and odd respectively. Therefore, multiply and integrating the functions together will always result in zero.

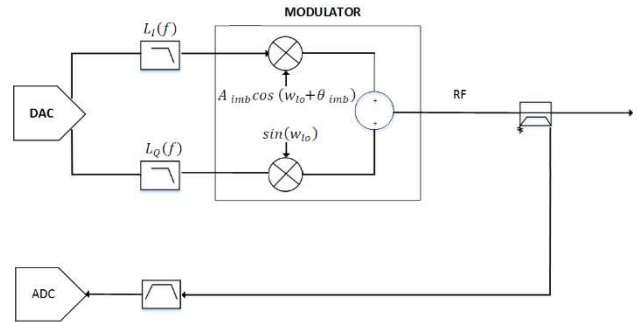


Fig. 10. Direct conversion transmitter with generic feedback path for adaptive correction

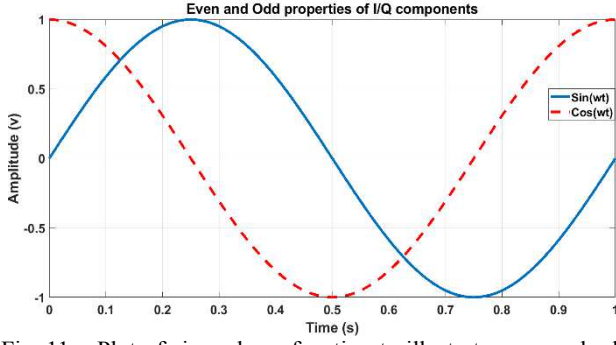


Fig. 11. Plot of sin and cos function to illustrate even and odd properties.

The orthogonality principle can be used to form the basis of the objective function,

$$Error = \int_{-l}^l I(t)Q(t)dt, \quad (24)$$

which minimization corresponds to I/Q imbalance estimation. The image suppression can be represented in terms of amplitude and phase imbalance by

$$IMRR(w) = \frac{G_{imb}(w)^2 + 1 - 2G_{imb}(w)\cos(\phi_{imb}(w))}{G_{imb}(w)^2 + 1 + 2G_{imb}(w)\cos(\phi_{imb}(w))}. \quad (25)$$

As shown in Fig. 12, the IQ imbalance can be seen as convex in nature and thus suitable for optimization methods such as gradient descent algorithm [4]. The update estimate equations for gain and phase imbalances can be described as

$$\phi_{imb-new} = \phi_{imb-old} + \lambda_{phase} I(t)Q_{corr1}(t), \quad (26)$$

and

$$G_{imb-new} = G_{imb-old} + \lambda_{gain} [I(t)^2 - Q_{corr2}(t)^2] \quad (27)$$

where

$$Q_{corr1}(t) = Q(t) - \phi_{imb-new} I(t) \quad (28)$$

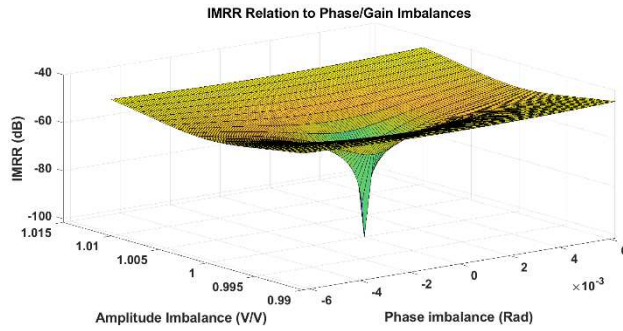


Fig. 12. IMRR as function of phase and amplitude imbalance

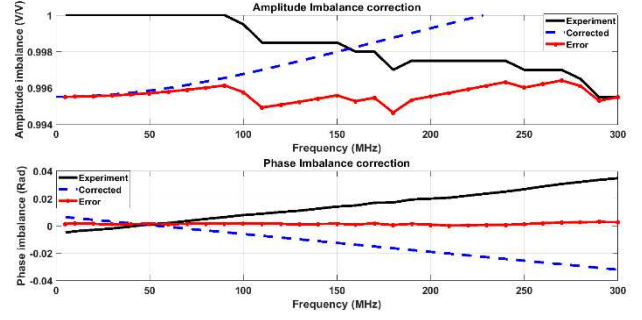


Fig. 13. Amplitude and phase correction of baseband IQ imbalances

and

$$Q_{corr2}(t) = G_{imb-new} Q_{corr1}(t). \quad (29)$$

λ_{gain} is the update gain for the amplitude imbalance error and λ_{phase} is the update gain for the phase imbalance error. The update gain variables should be chosen based on convergence of the corrections applied utilizing the corrective topology shown in Fig. 7.

VI. EXPERIMENTAL RESULTS

Amplitude and gain imbalances of a wideband transmitter were estimated by minimizing Eq. 25 with a spectrum analyzer at the output of transmitter for a variety of baseband offsets which the results are depicted in Fig. 13. Time delay corrections were applied utilizing a fractional delay filter and amplitude corrective topology as shown in Fig. 8. The corrective amplitude and phase is shown in Fig. 13, along with the resulting error remaining after the correction. Once the frequency corrections were estimated, a feedback calibration was performed to estimate wide-band IQ impairments. The phase and gain convergence curves for estimations are shown in Fig. 14.

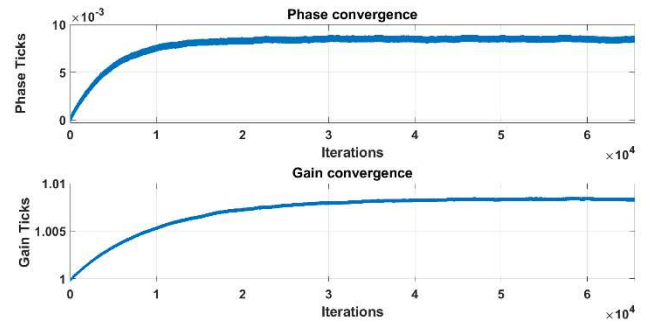


Fig. 14. Phase and gain estimates conversion using gradient decent algorithm

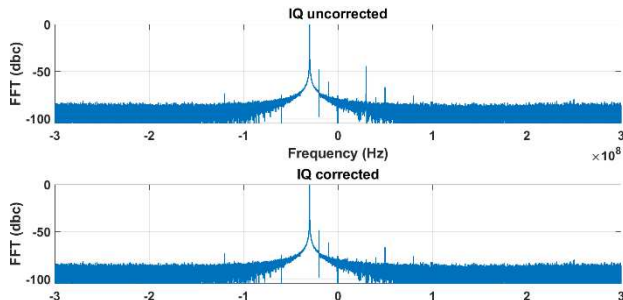


Fig. 15. Amplitude and phase correction of LO dependent IQ imbalances

The spectrum measured at the feedback of the ADC is shown in Fig. 15, before and after utilization of the gradient decent algorithm. It should be noted that IQ estimate algorithm is unbiased by spurs if there is not an associated image. If multiple tones or carriers are present, the algorithm will converge to the average IQ imbalance for all the carriers present. The spectrum of the transmitter output that generates multiple tones with only a single wide-band correction is shown in Fig. 16. Fig. 16 quite clearly demonstrate the frequency dependent nature of the imbalances and illustrates that a wideband correction by itself may be insufficient based on application. The combination of wideband and frequency dependent correction are shown in Fig. 17. The image suppression results over baseband frequencies are approaching -70 dBc. The results are suitable with margin for many radar and communication applications.

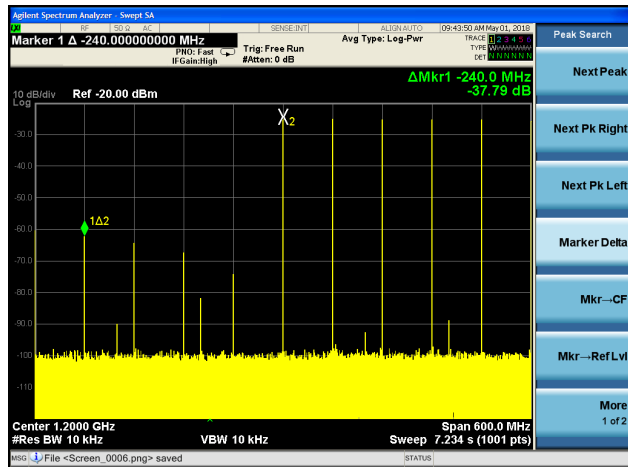


Fig. 16. Spectrum analyze capture of multi-tone transmitter with associative image tones using LO dependent or wideband correction

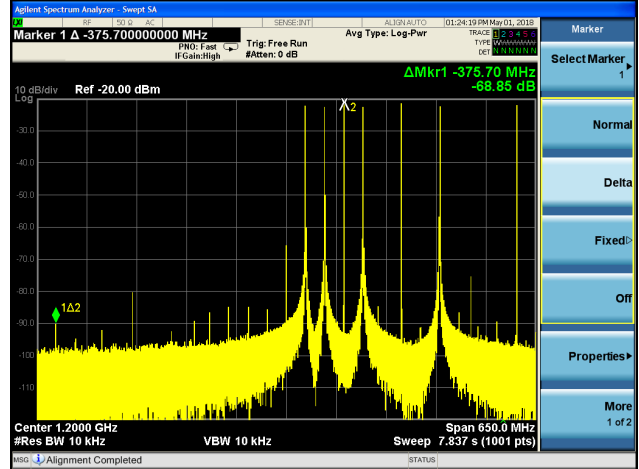


Fig. 17. Spectrum analyze capture of multi-tone transmitter with associative image tone using wideband and baseband frequency correction

VII. CONCLUSION

This paper depicted a root cause for the images in a direct conversion topology visually and mathematically. The amplitude and phase imbalances were separated into wideband dependent and baseband dependent components to allow for ease of correction and implementation of adaptive corrective topology. Estimation methods were shown utilizing gradient descent algorithm in a feedback topology. Experimental results were shown for gradient estimation method along with wideband and baseband corrective results based on feedback estimation and lab calibration respectively. The results of the correction are approaching -70 dBc of image suppression that are suitable for the majority of transmitter applications. Future work in this area will be to elaborate further on frequency domain corrective methodologies for non-well behaved IQ distortions with expansion to LO leakage correction.

REFERENCES

- [1] J.J Witt, 'Modelling, Estimation, and Compensation of Imbalances in Quadrature Transceivers', Stellenbosch University, 2011.
- [2] L. Hars, "Frequency Response Compensation with DSP", in Streamlining Digital Signal Processing 2nd Edition. Hoboken, NJ: Wiley, 2011, ch. 39.
- [3] V. Valimaki and T. I. Laakso, "Principles of fractional delay filters," 2000 IEEE International Conference on Acoustics, Speech, and Signal Processing. Proceedings (Cat. No.00CH37100), Istanbul, Turkey, 2000, pp. 3870-3873 vol.6.
- [4] 'IQ Correction', MEP Newsletter 3, 2011. [Online] Available:<http://www.delmar-north.com/microwave/requirements/IQGainPhaseCorrection.pdf>, [Accessed: Aug. 6, 2018]